

Research



**Cite this article:** Demuth OE, Wiseman ALA, Hutchinson JR. 2023 Quantitative biomechanical assessment of locomotor capabilities of the stem archosaur *Euparkeria capensis*. *R. Soc. Open Sci.* **10**: 221195.  
<https://doi.org/10.1098/rsos.221195>

Received: 13 September 2022

Accepted: 10 January 2023

**Subject Category:**

Organismal and Evolutionary Biology

**Subject Areas:**

palaeontology/biomechanics

**Keywords:**

locomotion, musculoskeletal modelling, Archosauria, bipedalism

**Authors for correspondence:**

Oliver E. Demuth

e-mail: [oed24@cam.ac.uk](mailto:oed24@cam.ac.uk)

John R. Hutchinson

e-mail: [jhutchinson@rvc.ac.uk](mailto:jhutchinson@rvc.ac.uk)

Electronic supplementary material is available online at <https://doi.org/10.6084/m9.figshare.c.6398135>.

# Quantitative biomechanical assessment of locomotor capabilities of the stem archosaur *Euparkeria capensis*

Oliver E. Demuth<sup>1,2</sup>, Ashleigh L. A. Wiseman<sup>1,3</sup> and John R. Hutchinson<sup>1</sup>

<sup>1</sup>Structure and Motion Laboratory, Department of Comparative Biomedical Sciences, The Royal Veterinary College, Hatfield, UK

<sup>2</sup>Department of Earth Sciences, and <sup>3</sup>McDonald Institute for Archaeological Research, University of Cambridge, Cambridge, UK

OED, 0000-0003-4876-1311; ALAW, 0000-0002-9575-4387; JRH, 0000-0002-6767-7038

Birds and crocodylians are the only remaining members of Archosauria (ruling reptiles) and they exhibit major differences in posture and gait, which are polar opposites in terms of locomotor strategies. Their broader lineages (Avenmetatarsalia and Pseudosuchia) evolved a multitude of locomotor modes in the Triassic and Jurassic periods, including several occurrences of bipedalism. The exact timings and frequencies of bipedal origins within archosaurs, and thus their ancestral capabilities, are contentious. It is often suggested that archosaurs ancestrally exhibited some form of bipedalism. *Euparkeria capensis* is a central taxon for the investigation of locomotion in archosaurs due to its phylogenetic position and intermediate skeletal morphology, and is argued to be representative of facultative bipedalism in this group. However, no studies to date have biomechanically tested if bipedality was feasible in *Euparkeria*. Here, we use musculoskeletal models and static simulations in its hindlimb to test the influences of body posture and muscle parameter estimation methods on locomotor potential. Our analyses show that the resulting negative pitching moments around the centre of mass were prohibitive to sustainable bipedality. We conclude that it is unlikely that *Euparkeria* was facultatively bipedal, and was probably quadrupedal, rendering the inference of ancestral bipedal abilities in Archosauria unlikely.

## 1. Introduction

Shifts in locomotor modes and postures, from quadrupedal to bipedal, or vice versa, were pivotal in the evolution of

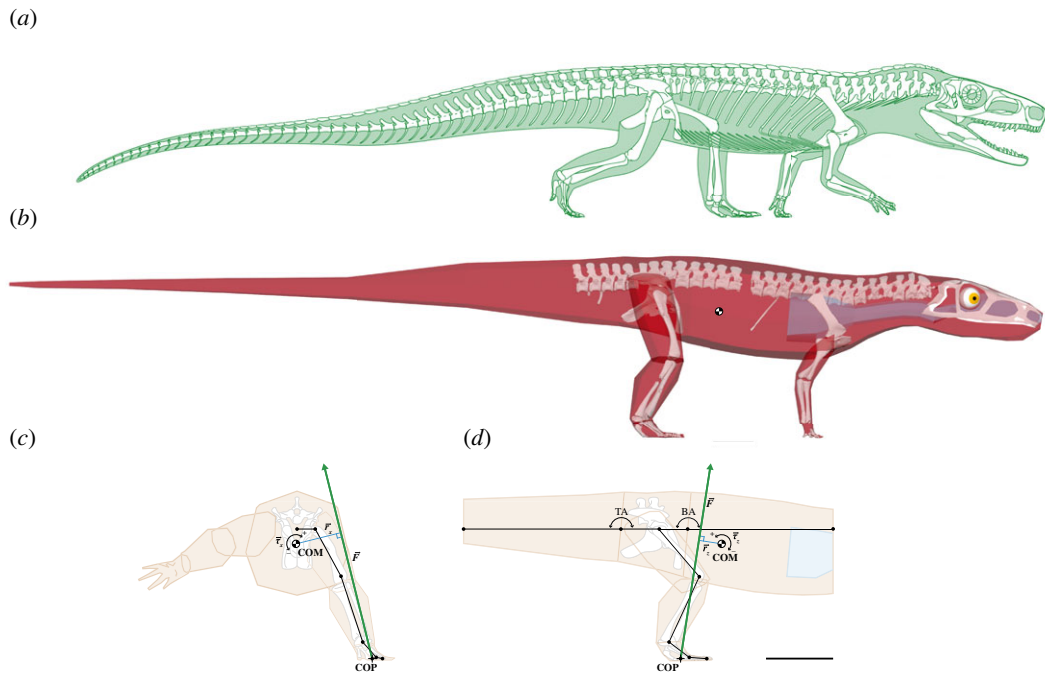


**Figure 1.** *Euparkeria* model. (a) Skeletal reconstruction of *Euparkeria capensis*, modified from Cuff *et al.* [27]. (b) Articulated digital skeleton of *Euparkeria* and hull and cavity models used for centre of mass (COM) (crossed circle) and inertia calculations. Modelled body posture and ground reaction force (GRF) vector in caudal view (c) and right lateral view (d). The body segments are shown in orange and the body cavities (lung, trachea, cranial sinus/pharynx) in blue; dots denote modelled joint centres. Note that the COM is cranial to both the hip joint and the GRF vector.  $r_x$  and  $r_z$ , respectively, represent the roll and pitch moment arms of the GRF vector  $F$  about the COM, producing the COM roll and pitch moments  $\tau_x$  and  $\tau_z$ . COM, centre of mass; COP, centre of pressure; BA, body angle; TA, tail angle. Angle deviations in the body and tail were measured from horizontal. All drawings to scale, scale bar = 5 cm.

tetrapods [1–6]. While these postural shifts are relatively rare, bipedalism has evolved independently in Squamata and Mammalia, and multiple times within Archosauria [1,5,7–10]. Birds and crocodylians, the last surviving lineages of Archosauria, are polar opposites in terms of posture and gait, the former being a habitual and erect biped and the latter a quadruped with a more sprawling-type gait [11–20]. However, throughout their evolutionary history, the two archosaurian clades Avemetatarsalia and Pseudosuchia explored a multitude of different locomotor modes [21–27], including multiple occurrences of bipedalism, such as their independent acquisition in pseudosuchians (i.e. poposaurids and shuvosaurids) and *Postosuchus*, and in Avemetatarsalia perhaps in lagerpetids and pterosauroforms, such as *Scleromochlus* [9,10,28–31]. The abundant fossil record of archosaurs facilitates detailed studies of their morphological and locomotor evolution [2,21,31–33]. However, the exact timing and frequency of the emergence of a more upright gait and bipedalism remain contentious [2,10,21,25–27,31,34,35].

The early archosauriform *Euparkeria capensis* from the Middle Triassic of South Africa [33,36] is a key taxon for disentangling the early locomotor evolution of archosaurs due to its plesiomorphic skeletal morphology, i.e. small-bodied, gracile, terrestrial and cursorial (see [37]; figure 1a), with a presumed posture that was intermediate between that of earlier, sprawling taxa and the fully erect stance seen in later taxa [25–27,37]. Together, these traits resemble the expected ancestral body plan for Archosauria [36–38]. This ancestral form and function are further supported by its stable phylogenetic position as sister taxon to Archosauria in both Bayesian and parsimony-based analyses [37,39]. The exact locomotor mode of *Euparkeria* has been a subject of debate. It has been classified as a facultative biped [9,24,33,40], mainly based on limb proportions. Contrastingly, other studies have instead classified *Euparkeria* as a habitual quadruped [10,30] with a relatively sprawling posture based on skeletal forelimb [41], hindlimb and ankle morphology [33,42], or alternatively with a more erect limb posture due to the similarity of the hindlimb bones and joints with those of crocodylians [21,22,43] or quantitative and functional analyses of the hindlimbs [26]. While joint mobility of its hindlimbs [26] or its muscle leverage in a comparative context [27] has been investigated, the locomotor performance of *Euparkeria* remains to be quantitatively tested.

Herein, we aim to overcome previous qualitative locomotory reconstructions, based on limb bone morphologies and their comparisons with potentially (but not necessarily) analogous taxa and/or

somewhat ambiguous assessments solely based on limb proportions, using quantitative and biomechanical principles. Musculoskeletal models can provide valuable insights into musculoskeletal function, which cannot otherwise be directly measured in physical experiments [20,44], and have become an increasingly popular tool in palaeobiology to estimate locomotor function and biomechanics [27,44–46]. A holistic approach, combining musculoskeletal modelling and other biomechanical tools, such as mechanical modelling of pitch moments around the centre of mass (COM) (e.g. [47,48]), enables the testing of bipedal capabilities in *Euparkeria*.

Forward acceleration generates a pitch moment around the COM and lifts the forelimbs off the ground, thus inducing bipedal postures, and that acceleration ends as soon as the velocity becomes constant and, consequently, the pitch moment dissipates [47,49]. Acceleration-induced bipedalism is, therefore, inherently unsustainable. By contrast, recent theoretical and experimental studies have shown that temporal asymmetry in the ground reaction force (GRF), in which the vertical component is skewed so that higher forces are exerted early in the stance phase, play a crucial role in achieving steady bipedal locomotion in birds and lizards [8,15,48,49], because their COM is situated cranial to the hips. An early skewed GRF profile increases the total amount of force that is applied along a resultant vector cranial to the COM during a stride, resulting in a larger nose-up pitch moment around the hips [8,48,49]. Additionally, angular acceleration of the trunk and tail about the hips are important factors in destabilizing quadrupedalism and facilitating bipedal locomotion instead [1,48]. Other forces such as aerodynamic lift play only a minor, effectively negligible role [49].

Here, we used musculoskeletal modelling and static simulations to investigate the bipedal capabilities of *E. capensis* and to test (i) if this species could have sustained a peak GRF expected during bipedal locomotion, and (ii) if the pitching moment about the COM facilitated sustainable bipedal locomotion. We then revisit the potential stance (habitually quadrupedal, facultatively or habitually bipedal) of ancestral Archosauria in light of our conclusions.

## 2. Material and methods

### 2.1. Model creation

The digital skeleton of *E. capensis* was assembled as composite of four  $\mu$ CT-scanned specimens (table 1) which were scaled to the holotype SAM PK 5867, the most complete specimen [26,33]. The bones were segmented in AVIZO 9.7 LITE (Thermo Fisher Scientific Inc., Waltham, MA, USA; <https://www.thermofisher.com/uk/en/home/electron-microscopy/products/software-em-3d-vis/avizo-software.html>) and MATERIALISE MIMICS 22.0 (Materialise NV, Leuven, Belgium; <https://www.materialise.com/en/healthcare/mimics-innovation-suite/mimics>) and rearticulated in a standard reference pose [16,50,51] in AUTODESK MAYA 2019 (Autodesk Inc., San Rafael, CA, USA; <https://www.autodesk.com/products/maya/overview>) following anatomical and joint coordinate system creation using geometric primitive shape-fitting [26,50,51]. The majority of the tail is not preserved in any of the  $\mu$ CT-scanned specimens of *Euparkeria*; it was, therefore, reconstructed based on photographs of several additional specimens (table 1; electronic supplementary material, figure S1). The model was posed in an osteologically feasible posture [26] for body segment modelling and COM estimation [50,52,53] and volumetric muscle creation [54,55] (figure 1*b*). We used a previously published three-dimensional musculoskeletal reconstruction of *Euparkeria* [27,55], which is briefly described here. Muscle origins and insertions were identified based on muscle scarring the extant phylogenetic bracket (EPB) [56,57] in combination with ancestral state reconstruction for ambiguous muscles following Bishop *et al.* [50] (see electronic supplementary material, figure S2 for muscle map). *Euparkeria* was, therefore, rescored based on new observations in the revised matrix [50] for osteological correlates of hindlimb musculature initially outlined by Hutchinson [58] and ambiguous muscle states reconstructed via maximum-parsimony analysis in MESQUITE 3.40 [59] (<http://www.mesquiteproject.org>). Volumetric muscles were subsequently created in AUTODESK MAYA 2019, constrained by tomographic sections of alligator hindlimbs [55] due to their similarity in limb morphology and proportions [33] and evolutionarily conserved myology [55], and their lines of action estimated following previously established protocols [20,55,60].

### 2.2. Musculoskeletal simulations

GRFs and body segment orientations were directly informed by the kinetics and kinematics of lizards [49,61–63]. This is unlike previous studies, for which the GRF was directed vertically from exactly

**Table 1.** Specimen list. See Demuth *et al.* [26] for  $\mu$ CT scan parameters. Multiple specimens of *Euparkeria* are preserved on slab SAM PK K8050 and two of them have the proximal caudal vertebrae preserved in articulation (see electronic supplementary material, figure S1). Institutional abbreviations: SAM, Iziko South African Museum, Cape Town, South Africa; IFGT, Institute for Geosciences, Eberhard-Karls-Universität Tübingen, Tübingen, Germany (formerly Geologisch-Paläontologisches Institut Tübingen: GPIT); UMZC, University Museum of Zoology Cambridge, Cambridge, UK.

$\mu$ CT-scanned specimens		specimen photographs	
specimen	elements	specimen	elements
SAM PK 5867	full body	SAM PK K8050 (1)	caudal vertebrae
SAM PK 6047A	pelvic girdle and forelimbs	SAM PK K8050 (2)	caudal vertebrae
SAM PK K8309	hindlimbs	SAM PK 13666	caudal vertebrae
UMZC T.692	fore and hindlimbs	GPIT 1686.1	caudal vertebrae

underneath the COM during mid-stance (e.g. [45,46,50]); however, this was not feasible because of the less erect hindlimb posture of *Euparkeria* (see [26]). Additionally, considering the asymmetrical GRFs in extant bipedally running lizards that peak during early stance phase [48], here it was assumed that the GRF profile for a bipedal *Euparkeria* would also have peaked during early stance. The hindlimb poses were configured accordingly and the GRF was thus applied to the centroid of the contact area (COP; figure 1c, d) of the right foot during early stance for the static simulations (no dynamic movement was modelled, see below). The assumed limb orientation was informed by data for the early stance phase in bipedally running lizards, using running kinematics of *Dipsosaurus dorsalis* and *Callisaurus draconoides* [61] (see electronic supplementary material, information S4 for joint angles). The GRF vector was adopted from empirical data collected by Sheffield *et al.* [62] and thus aimed 14° medially and 8° cranially (figure 1c,d). To test if *Euparkeria* could sustain GRFs expected during bipedal locomotion and how the body postures influenced the resulting muscle activations and pitch moments around the COM, several simulations and musculoskeletal models were set up. To cover the full breadth of possible bipedal body postures, the trunk and tail angles were each rotated by 0°, 25°, 50° and 75° (from horizontal to almost vertical), resulting in 16 simulations with varying combinations of trunk and tail angles (see [49]).

The models each had 16 active degrees of freedom, three rotational (pitch, yaw and roll) and three translational d.f. in the pelvis, three rotational d.f. (flexion/extension, abduction/adduction and long-axis rotation) in the hip and one d.f. (flexion/extension) each in the knee, ankle and metatarsophalangeal joints, and two d.f. (pitch and yaw) in both the proximal and mid-tail joints. Additionally, there were a total of three fixed (locked) d.f. per model: one d.f. (pitch) each in the trunk, neck and head joints.

To test the sensitivity of the architectural muscle parameters on the simulation results, four OPENSIM [64] (<https://simtk.org/projects/opensim>) musculoskeletal models were created using different estimation methods for muscle parameters (maximal isometric force  $F_{\max}$  and optimal fibre length  $l_0$ ): Model 1, alpha shape centroid; Model 2, convex hull centroid; and Model 3, arithmetic centroid; all following Bishop *et al.* [50] using previously published saurian muscle architectural data [55,65–67] representing the EPB [56,57]. Model 4 was generated from three-dimensional volumetric muscle models following Demuth *et al.* [55] (see electronic supplementary material, informations S1 and S2 for all muscle parameters). The muscle parameters were normalized and scaled by body mass [67–69], rather than segment or muscle tendon unit length [50], for data comparability. For the 16 static inverse simulations in OPENSIM 3.3 [64], the magnitude of the GRF was systematically increased for each pose until the static optimization algorithm could no longer find a solution to achieve static equilibrium for any combination of muscle activations ( $a_m$ ), while minimizing the sum of squared activations (see [50]),

$$\min \left( \sum_{m=1}^N a_m^2 + \sum_{q=1}^Q a_q^2 \right), \quad (2.1)$$

$$\text{subject to } \sum_{i=1}^n F_i \cdot r_{i,k} + M_{r,k} = M_k \quad (2.2)$$

and

$$F_i = a_i \cdot F_{\max,i}, \quad (2.3)$$

for each degree of freedom  $k$  ( $=16$ ). There were  $N = 36$  muscles (electronic supplementary material, figure S2 and information S2) and  $Q = 5$  reserve actuators in each model (one at the metatarsophalangeal joint

(flexion/extension) and two each in the proximal and mid-tail joints (roll and yaw)). The maximal torques of these reserve actuators are inconsequential as long as they are sufficiently large enough to never be fully activated [45,50]. Muscle force  $F_i$  was modelled as the product of activation and  $F_{\max}$ , while ignoring any intrinsic force–length–velocity relationships [50] (electronic supplementary material, information S2). The moment each muscle produced about a given degree of freedom was the product of its force  $F_i$  and its moment arm  $r_{i,k}$ . In total, 64 static simulations were computed, each testing a combination of the four different joint poses for both the tail and body and the different muscle parameter estimation methods in the four models.

The resulting muscle activations were interpolated at  $1^\circ$  intervals between the four different body postures per model, using cubic spline interpolation in MATLAB 2020a (The MathWorks, Inc., Natick, MA, USA; <https://www.mathworks.com/products/matlab.html>) to produce full coverage of the simulation space. Tail orientation had no influence on muscle activation and was, therefore, omitted.

### 2.3. COM moment calculations

The pitching moments around the COM were determined using the geometric definition of the moment arm as being the shortest perpendicular distance between a force's line of action and a centre of rotation [70], i.e. the COM position. Each moment was calculated as the shortest distance between two skew lines: the GRF vector from the COP in the foot and the unit vectors from the COM position representing its principal axes (figure 1c,d), and scaled by the two-dimensional projection of that distance onto each axis's plane of rotation [71], i.e. using its vector components (electronic supplementary material, information S3). The COM moments  $\tau$  were then calculated as the cross product of the moment arm  $r$  and the GRF  $F$  with a magnitude of 2 body weights (BW),

$$\tau = r \times F. \quad (2.4)$$

The moments around the COM were interpolated at  $1^\circ$  intervals between the 16 different simulations using cubic spline interpolation in MATLAB 2020a to cover the full range of tested postures.

The body segment orientations of six extant lizard species during bipedal locomotion were qualitatively compared with *Euparkeria* to relate their postural diversity to the pitching moments computed for *Euparkeria*. Data for lizards were gathered from Olberding *et al.* [63] for *Aspidoscelis sexlineata*, Irschick & Jayne [61] for *Callisaurus draconoides*, *Cnemidophorus tigris*, *Dipsosaurus dorsalis* and *Uma scoparia*, and van Wassenbergh & Aerts [49] for *Ctenophorus cristatus*.

### 2.4. Ancestral state reconstruction

The evolution of bipedalism within Archosauria was further investigated based upon two hypotheses regarding their interrelationship: the first phylogenetic tree, termed 'Nesbitt tree' followed work by Nesbitt [72], Nesbitt *et al.* [73], von Baczko *et al.* [74], Ezcurra *et al.* [75] and Foffa *et al.* [31], and the second, alternative tree, termed 'Ezcurra tree' was based on recent work by Ezcurra [76], Garcia *et al.* [77] and Müller & Garcia [78]. The phylogenetic trees were computed in the open-source software R [79] using the function 'DatePhylo' in the 'strap' package [80] and ancestral states were computed using different maximum-likelihood models, following Grinham *et al.* [9] in the R packages 'ape' [81] and 'phytools' [82]. The character states of the individual taxa were defined following [10,50]. The tips for the ambiguous taxa, i.e. *Hesperosuchus*, Pterosauria, Lagerpetidae, *Scleromochlus* and Silesauridae, were additionally estimated using the different models with their priors set to 0.5 for two character states (quadrupedal, bipedal) and 0.333 for the models with three character states (quadrupedal, facultatively bipedal, bipedal). For the latter, the transition matrices were manually set to ensure that the character states were ordered (from quadrupedal to facultatively bipedal to bipedal and vice versa). The most likely model was then chosen based on the Akaike information criterion (AIC) [83]. See electronic supplementary material, data for the R code and data.

## 3. Results

### 3.1. Pitch moments

Most of *Euparkeria*'s mass was concentrated in front of the hips, and the effects of changes in the static, plausible tail angles on the pitch moment mostly were negligible (s.d.  $\pm 0.014$  Nm; figure 2),



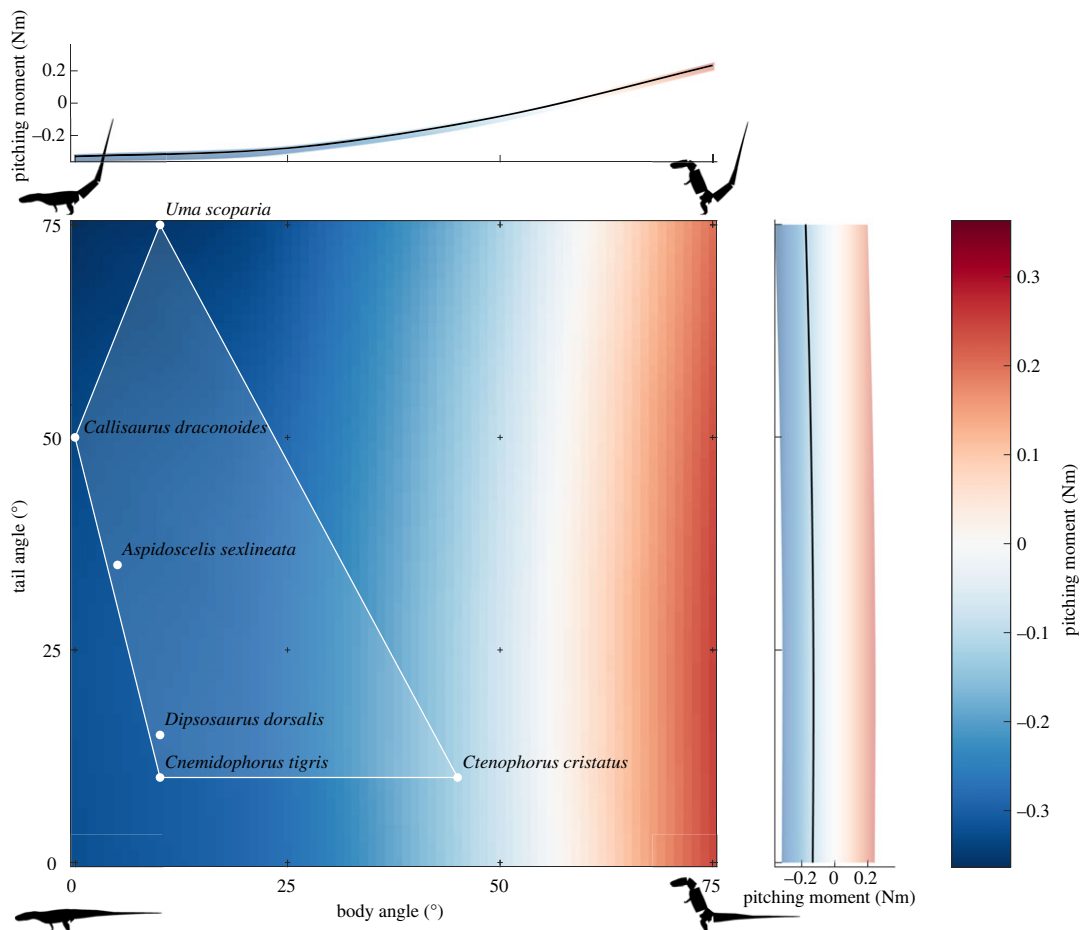


**Figure 2.** Pitching moment around the COM of *Euparkeria* during early stance and asymmetrical GRF. The black silhouettes qualitatively describe the body orientations of *Euparkeria* at the extreme points of the simulations. Body and tail postures of six extant lizards during bipedal locomotion are illustrated as circles and the posture space they occupy is indicated by the white transparent convex hull. Positive pitching moments (nose-up) are red, while negative pitching moments (nose-down) are blue. Note that bipedal poses similar to extant lizards resulted in a negative pitching moment around the COM for *Euparkeria*. Crosses denote simulation results; the values in between were interpolated at  $1^\circ$  intervals. The top and side plots display the range and average of pitching moments in relation to the body and tail angles, respectively.

whereas increase of the body angle shifted the COM towards the hips and substantially influenced the pitch moments (s.d.  $\pm 0.175$  Nm; figure 2). The magnitude of the negative pitching moment (nose-down) decreased with increasing body angle, until it switched sign, approximately at a body angle of  $60^\circ$ , and then subsequently increased again. The calculated pitch moments ranged from  $-0.363$  Nm in the posture with a  $0^\circ$  body angle and  $75^\circ$  tail angle, forcing the COM cranially (nose-down), to  $0.246$  Nm where the body and tail angles were  $75^\circ$  and  $25^\circ$ , respectively, forcing the COM caudally and dorsally (nose-up; figure 2). The six extant bipedal lizards all occupied postures with a large negative pitch moment for *Euparkeria* (figure 2). Only the posture of *Ctenophorus cristatus*, which has a more inclined body, approached a more neutral pitch moment; albeit still negative.

Sensitivity testing the modelling assumptions for the COM calculations, modifying the body segment shapes by  $\pm 20\%$  [52,53,84] and pushing the segment masses and their COM to implausible extremes [84], did not substantially influence our results (electronic supplementary material, figure S3 and information S3). The pitch moment around the COM stayed positive only for the implausible maximally caudal hull throughout the different body and tail orientations (electronic supplementary material, figure S3 and information S3). The overall mean across all hulls for the sensitivity analysis was consistent with the optimal hull, with a mean difference of the pitching moments of only 4.85% (electronic supplementary material, information S3), indicating that the optimal hull (as presented in figure 2) best represented the body proportions and mass properties of *Euparkeria*.

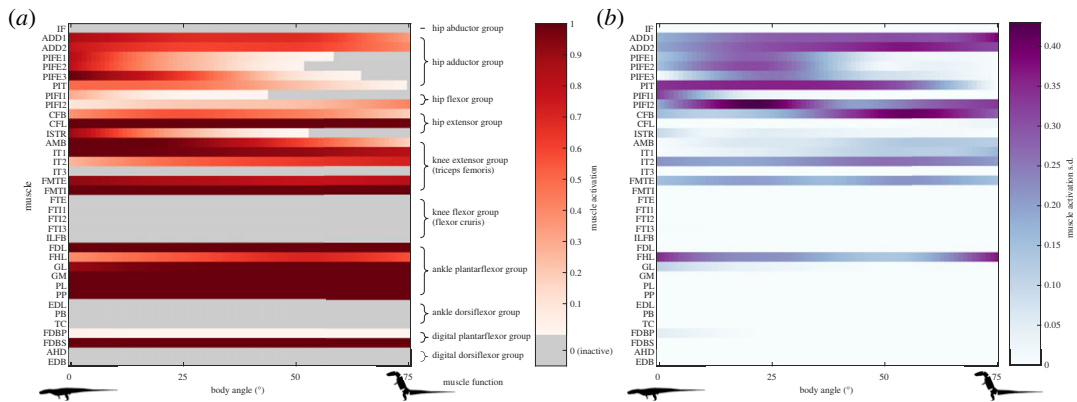


**Figure 3.** Mean activation (*a*) and its corresponding standard deviation (*b*) of the *Euparkeria* muscles across all models and simulations at their maximally sustainable GRF. Tail angle had no influence on muscle activation. Mean muscle activation was calculated at 0°, 25°, 50° and 75°; the values in between were interpolated at 1° intervals. The distal hindlimb muscle homologies follow Hattori & Tsuihiji [85]. See electronic supplementary material, figure S4 for the muscle activation of the individual models. IF, M. iliofemoralis; ADD 1–2, M. adductor femoris 1 + 2; PIFE1–3, M. puboischiofemoralis externus 1–3; PIT, M. puboischiotibialis; PIFI1–2, M. puboischiofemoralis internus 1–2; CFB, M. caudofemoralis brevis; CFL, M. caudofemoralis longus; ISTR, M. ischitrochantericus; AMB, M. ambiens; IT1–3, M. ilirotibialis 1–3; FMTE, M. femorotibialis externus; FMTI, M. femorotibialis internus; FTE, M. flexor tibialis externus, FTI1–3, M. flexor tibialis internus 1–3; ILFB, M. iliofibularis; FDL, M. flexor digitorum longus; FHL, M. flexor hallucis longus; GL, M. gastrocnemius lateralis; GM, M. gastrocnemius medialis; PL, M. peroneus (fibularis) longus; PP, M. pronator profundus; EDL, M. extensor digitorum longus; PB, M. peroneus (fibularis) brevis; TC, M. tibialis cranialis; FDBP, M. flexor digitorum brevis profundus; FDBS, M. flexor digitorum brevis superficialis; AHD, M. adductor hallucis dorsalis; EDB, M. extensor digitorum brevis.

### 3.2. Muscle activation

The patterns in hindlimb muscle activations at peak GRF were roughly similar between the different simulations (figure 3; table 2; electronic supplementary material, figure S4). These muscle activation patterns generally fall within predicted ranges (see [50]). Muscles that counteract gravitational forces, e.g. the ankle plantarflexors, the knee extensors, the hip extensors and to some degree the hip adductors, were highly activated, while the antagonistic flexor muscles remained mostly inactive. The variation and discrepancy between the different simulations were highest among the pelvic muscles (figure 3*b*), mainly caused by Model 4, which had very high muscle activations in the adductor muscle group at low body angles, and additionally high activation in the hip flexor muscles, which were mostly inactive in the other models. Those activations were far less pronounced in the other simulations (table 2; electronic supplementary material, figure S4). In addition to the ankle plantarflexor muscles, the knee extensor muscles were also maximally recruited in Model 3, even surpassing the muscle activation of the ankle plantarflexors. Overall, the highest activations were observed in the ankle plantarflexor group, which was the ‘weak link’ in the simulations (figure 3*a*). A further increase of the GRF by 0.1 BW resulted in failure of those muscles and the collapse of the ankle joint in all simulations (see electronic supplementary material, table S1 for hind limb joint moments).

Changes in body angle mainly influenced the hip adductor and hip extensor muscle group activations. Alongside an increased body angle, the COM was located more caudally towards the pelvis, reducing its moment arm about the hip joint and thus becoming less demanding on those two muscle groups. Interestingly, an increase in the body angle shifted the muscle activation in the hip flexor group from PIFI1 to PIFI2 in all simulations; however, their activations remained relatively low overall (figure 3; electronic supplementary material, figure S4).

Due to the larger estimated muscle masses based on the three-dimensional models (electronic supplementary material, information S2) and the resultant associated  $F_{\max}$  in Model 4, the sustained GRF was between 130% and 145% greater than in the other three models (table 2), for which the muscle parameters were solely estimated using scaled architectural muscle data from extant Sauria.

### 3.3. Evolution of bipedalism within Archosauria

The ancestral state reconstructions for both tree topologies were very similar (figure 4) and the results were thus relatively robust to differing hypotheses about their interrelationships or uncertainties in the

**Table 2.** Mean muscle activations per muscle group at maximal sustainable GRF. IT3 was excluded from knee extensors, because it acted mainly as knee abductor and knee flexor in the *Euparkeria* model and therefore was inactive during the simulations. Note that the 'weak link' was the ankle joint in most simulations; additionally, in Model 3 the knee extensors reached their limit and in Model 4 the hip adductors. abd., abductors; add., adductors; flex., flexors; ext., extensors; plan., plantar flexors; dorsi., dorsiflexors; dig., digital.

muscle groups	Model 1 (alpha shape centroid)				Model 2 (convex hull centroid)				Model 3 (arithmetic centroid)				Model 4 (three-dimensional model)			
	0	25	50	75	0	25	50	75	0	25	50	75	0	25	50	75
hip abd.	0.000	0.000	0.000	0.000	0.000	0.000	0.000	0.000	0.000	0.000	0.000	0.007	0.000	0.000	0.000	0.000
hip add.	0.624	0.302	0.144	0.052	0.762	0.334	0.193	0.081	0.765	0.415	0.282	0.076	1.000	0.901	0.494	0.287
hip flex.	0.090	0.020	0.021	0.060	0.069	0.000	0.046	0.090	0.041	0.000	0.268	0.413	0.724	0.431	0.131	0.273
hip ext.	0.718	0.559	0.395	0.331	0.801	0.633	0.460	0.362	0.790	0.679	0.667	0.532	0.727	0.574	0.400	0.333
knee ext.	0.773	0.755	0.695	0.638	0.891	0.870	0.801	0.743	0.885	0.954	0.957	0.853	0.800	0.859	0.692	0.588
knee flex.	0.000	0.000	0.000	0.000	0.000	0.000	0.000	0.000	0.000	0.000	0.000	0.000	0.000	0.000	0.000	0.000
ankle plan.	0.954	0.954	0.954	0.954	0.938	0.938	0.938	0.938	0.834	0.863	0.927	0.840	0.792	0.941	0.980	0.980
ankle dorsi.	0.000	0.000	0.000	0.000	0.000	0.000	0.000	0.000	0.000	0.000	0.000	0.000	0.000	0.000	0.000	0.000
dig. plan.	0.502	0.503	0.502	0.502	0.502	0.503	0.502	0.502	0.502	0.502	0.503	0.503	0.705	0.503	0.502	0.502
dig. dorsi.	0.000	0.000	0.000	0.000	0.000	0.000	0.000	0.000	0.000	0.000	0.000	0.000	0.000	0.000	0.000	0.000
max GRF [BW]	2.9	2.9	2.9	2.9	3.0	3.0	3.0	3.0	2.9	3.0	3.1	3.0	6.7	7.3	7.4	7.4



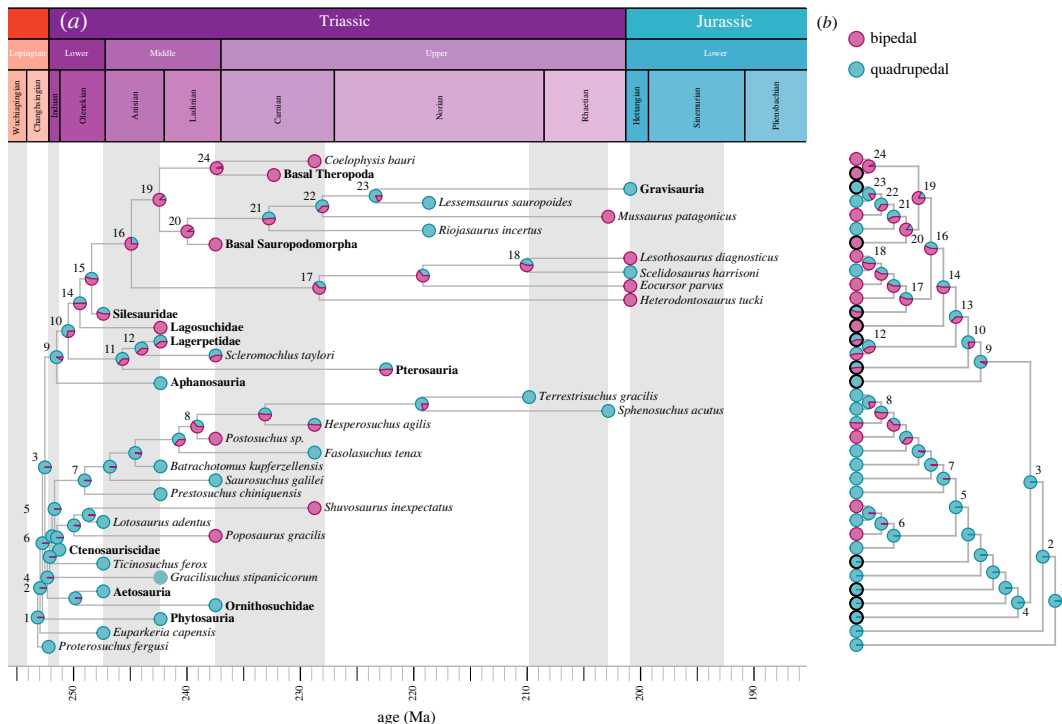


**Figure 4.** Evolution of bipedalism within Archosauria. Ancestral state reconstruction for the time-calibrated ‘Nesbitt tree’ (a) and ‘Ezcurra tree’ (b); see methods for sources of tree topologies; see electronic supplementary material, figures S5–S8 for individual time-calibrated trees. Red circles indicate bipedalism and blue circles indicate quadrupedalism; black outlined circles in (b) represent the bold clades in (a). Clades: 1, Archosauriformes; 2, Eucrocopoda; 3, Archosauria; 4, Pseudosuchia; 5, Paracrocodylomorpha; 6, Poposauroida; 7, Loricata; 8, Crocodylomorpha; 9, Avemetatarsalia; 10, Ornithodira; 11, Pterosauroomorpha; 12, Lagerpetidae; 13, Dinosauromorpha; 14, Dinosauriformes; 15, Dracohors; 16, Dinosauria; 17, Ornithischia; 18, Neornithischia; 19, Saurischia; 20, Sauropodomorpha; 21, Massopoda; 22, Sauropodiformes; 23, Sauropoda; 24, Theropoda.

tree topologies. Two character states with an ‘equal rates’ model were considered to be the most likely based on AIC values (49.69 for the ‘Nesbitt tree’ and 49.71 for the ‘Ezcurra tree’). For three character states an ‘unequal rates’ model with all rates different would have been the most likely (AIC 63.91 for the ‘Nesbitt tree’ and 63.54 for the ‘Ezcurra tree’); however, the models with three character states were all less likely than the models with only two character states (lower log-likelihood and larger AIC values; see electronic supplementary material, table S2).

Overall, Archosauria was consistently reconstructed as quadrupedal, and Pseudosuchia might have evolved bipedalism up to three times (perhaps twice in poposaurids; once in *Postosuchus*), all within the Ladinian–Carnian stages (Middle–Late Triassic). The estimation of Crocodylomorpha as ancestrally bipedal, however, might be an artefact of the short branch length leading to *Postosuchus* sp. In Avemetatarsalia, the emergence of bipedalism is somewhat ambiguous. It arose in the Olenekian, but there were some differences in the maximum likelihoods for its exact occurrence depending on the tree. Bipedalism arose once at the base of Dinosauriformes in the ‘Ezcurra tree’. Contrastingly, however, in the ‘Nesbitt tree’ it potentially emerged twice; firstly, in Dracohors, on the line leading to dinosaurs, and secondly, in parallel, in Lagosuchidae. Lagerpetids and pterosaurs consistently were estimated as quadrupedal, while the ambiguous Silesauridae was consistently estimated as ancestrally bipedal.

## 4. Discussion and conclusion

The hindlimb of *Euparkeria* was able to sustain the GRF expected during bipedal locomotion (greater than 2 BW) in all simulations, however, due to the large negative pitch moments around the COM at maximum GRF for most simulations, and especially in postures adopted by extant bipedal lizards (figure 2), it appears unlikely that *Euparkeria* habitually adopted bipedalism. To sustain bipedal locomotion, the angular momentum about the COM that is generated during each stride must be zero [15,47].

Temporal asymmetry in the GRF in birds and lizards, with higher forces exerted early in stance phase, enables steady bipedal locomotion, due to a larger nose-up pitch moment, resulting from a

larger amount of force that is applied along the resultant vector cranial to the COM during a stride [8,15,47,48], and their COM is situated cranial to the hips. Under the assumption of such an early skewed GRF profile, resulting in a larger nose-up pitch moment [8,48,49], the pitch moment at peak GRF for *Euparkeria* should have been positive or close to zero if it were bipedal. However, this was only possible at extreme body angles of greater than 60° in our simulations, unknown in any bipedal saurian. Of the six extant bipedal lizard taxa for which body postures have been reported, *Euparkeria* qualitatively matches the body proportions of *Callisaurus draconoides*, which has the most negative pitch moments (figure 2), most closely. *Euparkeria* is, however, significantly larger than any of the bipedal lizard taxa, and, unfortunately but also intriguingly, no modern analogue exists for *Euparkeria*.

We did not model any dynamic movement, such as forward acceleration [7,47] or rotational inertia and angular momentum of the body and tail [1,47,48,86], which help counteract the nose-down pitch moment caused by gravity. However, such dynamic assumptions may not change our conclusions, which were based solely upon static simulations. In particular, an acceleration causing a positive pitching moment that lifts the trunk and the forelimbs off the ground only occurs when speed is increasing. As soon as the animal reaches its maximal speed, the net propulsive impulse and the resulting pitching moment become zero [47] and gravity takes over—pushing the nose back down (gravity-induced negative pitch; figure 2). Purely acceleration-driven bipedal locomotion is, therefore, inherently unsustainable and cannot explain bipedal locomotion in extant lizards [7,49,63]; hence acceleration was disregarded in this study. Dynamic simulations which incorporate angular momentum, such as Bishop *et al.* [87], may provide an avenue for future investigation to decipher the evolution of bipedal locomotor capabilities within archosaurs. Regardless, our findings are in line with recent quantitative studies on femoral shape [10], femoral microanatomy [88] and body COM position [30], suggesting that *Euparkeria* was a habitual quadruped. We further support this conclusion from the point of view of musculoskeletal biomechanics.

Our results from the ancestral state reconstruction indicate that bipedalism evolved once, maybe twice, somewhere within Ornithodira; but at least twice in pseudosuchians (podosaurids, *Postosuchus*). While secondary quadrupedalism was common in Ornithodira; i.e. several groups of ornithischians [5] as well as in sauropods independently evolved quadrupedalism; Pseudosuchia may or may not have ever reverted back to quadrupedalism from a bipedal form as our results are currently ambiguous in that regard. Further quantitative testing of bipedalism in some of the ambiguous taxa, i.e. *Hesperosuchus*, *Scleromochlus* and/or silesaurids, is necessary to disentangle the evolution of bipedalism within Archosauria.

*Euparkeria* and other early archosauriforms lacked morphological and functional specializations related to bipedal movement, such as having a fully erect hindlimb and/or parasagittal gait [2,25,26]. Their pes was also more specialized for quadrupedal locomotion [26,89], which is unlike the elongated and mediolaterally compressed tarsus and pes seen in bipedal taxa [29,90]. Additionally, the femora of archosauromorphs, including both early avemetatarsalians and pseudosuchians, further suggest that this group had a habitually quadrupedal posture prior to and initially after the split into bird- and crocodile-line archosaurs [10]. Our functional and biomechanical analysis of the locomotor mode of *Euparkeria* goes beyond these primarily morphological studies. It demonstrates, and explains via Newtonian mechanics, that bipedalism could not be achieved with the body plan of early archosaurs. More specifically, our analysis has allowed for the testing of the potential locomotor behaviour of an extinct stem archosaur, pointing towards an answer to the controversy over how *Euparkeria* moved. Morphological changes in the pelvis and hindlimb of later pseudosuchians and ornithodirans facilitated a parasagittal gait, bipedalism and digitigrade foot orientation to independently evolve at some points [10,26,27,29]. Ancestral archosaurs, therefore, did not exhibit bipedalism (figure 4). Ornithodira and Pseudosuchia inherited a body plan from Archosauria that subsequently was modified in the aftermath of the Permo-Triassic mass extinction, enabling novel locomotor modes such as bipedalism to evolve independently.

**Data accessibility.** The datasets generated and/or analysed during the current study are included in this published article (and its electronic supplementary material, information files [91]). The OpenSim models and their corresponding simulation files, the R code and its files for the ancestral state reconstruction, and the *Euparkeria* pelvis, hindlimb and muscle models are available from the following figshare repository: <https://figshare.com/s/73c07f4c9b930c25a3f9>.

**Authors' contributions.** O.E.D.: conceptualization, formal analysis, investigation, methodology, validation, visualization, writing—original draft; A.L.A.W.: formal analysis, investigation, methodology, validation, writing—original draft; J.R.H.: conceptualization, formal analysis, funding acquisition, investigation, methodology, validation, writing—original draft.

All authors gave final approval for publication and agreed to be held accountable for the work performed therein.

Conflict of interest declaration. The authors declare no competing interest.

Funding. J.R.H. was supported by funding from the European Research Council (ERC) under the European Union's Horizon 2020 research and innovation programme (grant agreement 695517).

Acknowledgements. We thank Lucy Roberts and Matteo Fabbri for, respectively, sharing their segmented models of the presacral vertebrae and skull of *Euparkeria* SAM PK 5887. Additionally, we thank Roland Sookias and Richard Butler for providing photographs of several specimens of *Euparkeria* from the SAM and GPIT. We are grateful to Peter Bishop for his valuable input and insightful discussions that helped shape this paper. We further thank Matthew Lowe and Jason Head for collections and curatorial support at UMZC, Keturah Smithson for conducting the UMZC  $\mu$ CT scans, Claire Browning and Zaituna Skosan for collections and curatorial support at SAM and Stephan Le Roux for providing the  $\mu$ CT data of *Euparkeria* from the SAM. We thank three anonymous reviewers for their constructive feedback which improved the manuscript.

## References

- Snyder RC. 1962 Adaptations for bipedal locomotion of lizards. *Am. Zool.* **2**, 191–203. (doi:10.1093/icb/2.2.191)
- Sereno PC. 1991 Basal archosaurs: phylogenetic relationships and functional implications. *J. Vertebr. Paleontol.* **11**, 1–53. (doi:10.1080/02724634.1991.10011426)
- Gatesy SM, Middleton KM. 1997 Bipedalism, flight, and the evolution of theropod locomotor diversity. *J. Vertebr. Paleontol.* **17**, 308–329. (doi:10.1080/02724634.1997.10010977)
- Kubo T, Benton MJ. 2009 Tetrapod postural shift estimated from Permian and Triassic trackways. *Palaeontology* **52**, 1029–1037. (doi:10.1111/j.1475-4983.2009.00897.x)
- Barrett PM, Maidment SCR. 2017 The evolution of ornithischian quadrupedality. *J. Iber. Geol.* **43**, 363–377. (doi:10.1007/s41513-017-0036-0)
- Maher AE, Burin G, Cox PG, Maddox TW, Maidment SCR, Cooper N, Schachner ER, Bates KT. 2022 Body size, shape and ecology in tetrapods. *Nat. Commun.* **13**, 4340. (doi:10.1038/s41467-022-32028-2)
- Clemente CJ, Withers PC, Thompson G, Lloyd D. 2008 Why go bipedal? Locomotion and morphology in Australian agamid lizards. *J. Exp. Biol.* **211**, 2058–2065. (doi:10.1242/jeb.018044)
- Clemente CJ, Bishop PJ, Newman N, Hocknull SA. 2018 Steady bipedal locomotion with a forward situated whole-body centre of mass: the potential importance of temporally asymmetric ground reaction forces. *J. Zool.* **304**, 193–201. (doi:10.1111/jzo.12521)
- Grinham LR, VanBuren CS, Norman DB. 2019 Testing for a facultative locomotor mode in the acquisition of archosaur bipedality. *R. Soc. Open Sci.* **6**, 190569. (doi:10.1098/rsos.190569)
- Pintore R, Houssaye A, Nesbitt SJ, Hutchinson JR. 2022 Femoral specializations to locomotor habits in early archosauriforms. *J. Anat.* **240**, 867–892. (doi:10.1111/joa.13598)
- Gatesy SM. 1991 Hind limb movements of the American alligator (*Alligator mississippiensis*) and postural grades. *J. Zool.* **224**, 577–588. (doi:10.1111/j.1469-7998.1991.tb03786.x)
- Gatesy SM. 1995 Functional evolution of the hindlimb and tail from basal theropods to birds. In *Functional morphology in vertebrate paleontology* (ed. JJ Thomason), pp. 219–234. New York, NY: Cambridge University Press.
- Hutchinson JR, Gatesy SM. 2000 Adductors, abductors, and the evolution of archosaur locomotion. *Paleobiology* **26**, 734–751. (doi:10.1666/0094-8373(2000)026<0734:AAATEO>2.0.CO;2)
- Hutchinson JR. 2006 The evolution of locomotion in archosaurs. *C. R. Palevol* **5**, 519–530. (doi:10.1016/j.crpv.2005.09.002)
- Andrada E, Rode C, Sutedja Y, Nyakatura JA, Blickhan R. 2014 Trunk orientation causes asymmetries in leg function in small bird terrestrial locomotion. *Proc. R. Soc. B* **281**, 20141405. (doi:10.1098/rspb.2014.1405)
- Kambic RE, Roberts TJ, Gatesy SM. 2014 Long-axis rotation: a missing degree of freedom in avian bipedal locomotion. *J. Exp. Biol.* **217**, 2770–2782. (doi:10.1242/jeb.101428)
- Hutchinson JR, Felkner D, Houston K, Chang Y-M, Brueggen J, Kledzik D, Vliet KA. 2019 Divergent evolution of terrestrial locomotor abilities in extant Crocodylia. *Sci. Rep.* **9**, 19302. (doi:10.1038/s41598-019-55768-6)
- Allen VR, Kilbourne BM, Hutchinson JR. 2021 The evolution of pelvic limb muscle moment arms in bird-line archosaurs. *Sci. Adv.* **7**, eabe2778. (doi:10.1126/sciadv.abe2778)
- Wiseman ALA, Bishop PJ, Demuth OE, Cuff AR, Michel KB, Hutchinson JR. 2021 Musculoskeletal modelling of the Nile crocodile (*Crocodylus niloticus*) hindlimb: effects of limb posture on leverage during terrestrial locomotion. *J. Anat.* **239**, 424–444. (doi:10.1111/joa.13431)
- Bishop PJ, Michel KB, Falisse A, Cuff AR, Allen VR, De Groot F, Hutchinson JR. 2021 Computational modelling of muscle fibre operating ranges in the hindlimb of a small ground bird (*Eudromia elegans*), with implications for modelling locomotion in extinct species. *PLoS Comput. Biol.* **17**, e1008843. (doi:10.1371/journal.pcbi.1008843)
- Parrish JM. 1986 Locomotor adaptations in the hindlimb and pelvis of the Thecodontia. *Hunteria* **1**, 1–35.
- Parrish JM. 1987 The origin of crocodylian locomotion. *Paleobiology* **13**, 396–414. (doi:10.1017/S0094837300090903)
- Kubo T, Benton MJ. 2007 Evolution of hindlimb posture in archosaurs: limb stresses in extinct vertebrates. *Palaeontology* **50**, 1519–1529. (doi:10.1111/j.1475-4983.2007.00723.x)
- Kubo T, Kubo MO. 2012 Associated evolution of bipedality and cursoriality among Triassic archosaurs: a phylogenetically controlled evaluation. *Paleobiology* **38**, 474–485. (doi:10.1666/11015.1)
- Sullivan CS. 2015 Evolution of hind limb posture in Triassic archosauriforms. In *Great transformations in vertebrate evolution* (eds KP Dial, N Shubin, EL Brainerd), pp. 107–124. Chicago, IL: University of Chicago Press.
- Demuth OE, Rayfield EJ, Hutchinson JR. 2020 3D hindlimb joint mobility of the stem-archosaur *Euparkeria capensis* with implications for postural evolution within Archosauria. *Sci. Rep.* **10**, 15357. (doi:10.1038/s41598-020-70175-y)
- Cuff AR, Demuth OE, Michel K, Otero A, Pintore R, Polet DT, Wiseman ALA, Hutchinson JR. 2022 Walking—and running and jumping—with dinosaurs and their cousins, viewed through the lens of evolutionary biomechanics. *Integr. Comp. Biol.* **00**, 1–25. (doi:10.1093/icb/iciac049)
- Gauthier JA, Nesbitt SJ, Schachner ER, Bever GS, Joyce WG. 2011 The bipedal stem crocodylian *Poposaurus gracilis*: inferring function in fossils and innovation in archosaur locomotion. *Bull. Peabody Mus. Nat. Hist.* **52**, 107–126. (doi:10.3374/014.052.0102)
- Bates KT, Schachner ER. 2012 Disparity and convergence in bipedal archosaur locomotion. *J. R. Soc. Interface* **9**, 1339–1353. (doi:10.1098/rsif.2011.0687)
- Bishop PJ, Bates KT, Allen VR, Henderson DM, Randau M, Hutchinson JR. 2020 Relationships to mass properties and body proportions to locomotor habit in terrestrial Archosauria. *Paleobiology* **46**, 550–568. (doi:10.1017/pab.2020.47)
- Foffa D *et al.* 2022 *Scleromochlus* and the early evolution of Pterosauroomorpha. *Nature* **610**, 313–318. (doi:10.1038/s41586-022-05284-x)
- Brusatte SL, Benton MJ, Lloyd GT, Ruta M, Wang SC. 2010 Macroevolutionary patterns in the evolutionary radiation of archosaurs (Tetrapoda: Diapsida). *Earth Environ. Sci. Trans. R. Soc. Edinb.* **101**, 367–382. (doi:10.1017/S1755691011020056)
- Ewer RF. 1965 The anatomy of the thecodont reptile *Euparkeria capensis* Broom. *Phil. Trans. R. Soc. Lond. B* **248**, 379–435. (doi:10.1098/rstb.1965.0003)

34. Padian K, Li C, Pchelinkova J. 2010 The trackmaker of *Apatopus* (Late Triassic, North America): implications for the evolution of archosaur stance and gait. *Palaentology* **53**, 175–189. (doi:10.1111/j.1475-4983.2009.00924.x)
35. Brusatte SL, Niedzwiedzki G, Butler RJ. 2011 Footprints pull origin and diversification of dinosaur stem lineage deep into Early Triassic. *Proc. R. Soc. B* **278**, 1107–1113. (doi:10.1098/rspb.2010.1746)
36. Sookias RB, Butler RJ, Nesbitt SJ, Desojo JB, Irmis RB. 2013 Euparkeriidae. In *Anatomy, phylogeny and palaeobiology of early archosaurs and their kin* (eds SJ Nesbitt, JB Desojo, RB Irmis), pp. 35–48. London, UK: Geological Society.
37. Sookias RB. 2016 The relationships of the Euparkeriidae and the rise of Archosauria. *R. Soc. Open Sci.* **3**, 150674. (doi:10.1098/rsos.150674)
38. Sookias RB, Sullivan CS, Liu J, Butler RJ. 2014 Systematics of putative euparkeriids (Diapsida: Archosauriformes) from the Triassic of China. *PeerJ* **2**, e658. (doi:10.7717/peerj.658)
39. Sookias RB, Dilkes D, Sobral G, Smith RMH, Wolvaardt FP, Arcucci AB, Bhullar B-AS, Wernberg I. 2020 The craniomandibular anatomy of the early archosauriform *Euparkeria capensis* and the dawn of the archosaur skull. *R. Soc. Open Sci.* **7**, 200116. (doi:10.1098/rsos.200116)
40. Santi G. 1993 Functional bipedalism in some Permo-Triassic extinct reptiles: a possible scale of the degree of efficiency. *Stud. Trent. Sci. Nat. Acta Biol.* **68**, 267–280.
41. Remes K. 2007 Evolution of the pectoral girdle and forelimb in Sauropodomorpha (Dinosauria, Saurischia): osteology, myology and function. Dissertation, Ludwig-Maximilians-Universität München, Munich, Germany.
42. Sullivan CS. 2007 Function and evolution of the hind limb in Triassic archosaurian reptiles. PhD thesis, Harvard University, Cambridge, MA.
43. Paul GS. 2002 *Dinosaurs of the air: the evolution and loss of flight in dinosaurs and birds*. Baltimore, MD: Johns Hopkins University Press.
44. Demuth OE, Herbst EC, Polet DT, Wiseman ALA, Hutchinson JR. In press. Modern three-dimensional digital methods for studying locomotor biomechanics in tetrapods. *J. Exp. Biol.*
45. Bishop PJ, Hocknull SA, Clemente CJ, Hutchinson JR, Barrett RS, Lloyd DG. 2018 Cancellous bone and theropod dinosaur locomotion. Part II—a new approach to inferring posture and locomotor biomechanics in extinct tetrapod vertebrates. *PeerJ* **6**, e5779. (doi:10.7717/peerj.5779)
46. Bishop PJ, Hocknull SA, Clemente CJ, Hutchinson JR, Farke AA, Barrett RS, Lloyd DG. 2018 Cancellous bone and theropod dinosaur locomotion. Part III—inferring posture and locomotor biomechanics in extinct theropods, and its evolution on the line to birds. *PeerJ* **6**, e5777. (doi:10.7717/peerj.5777)
47. Aerts P, Van Damme R, D’Aout K, Van HB. 2003 Bipodalism in lizards: whole-body modelling reveals a possible spandrel. *Phil. Trans. R. Soc. Lond. B* **358**, 1525–1533. (doi:10.1098/rstb.2003.1342)
48. Clemente CJ, Wu NC. 2018 Body and tail-assisted pitch control facilitates bipedal locomotion in Australian agamid lizards. *J. R. Soc. Interface* **15**, 20180276. (doi:10.1098/rsif.2018.0276)
49. Van Wassenbergh S, Aerts P. 2013 In search of the pitching momentum that enables some lizards to sustain bipedal running at constant speeds. *J. R. Soc. Interface* **10**, 20130241. (doi:10.1098/rsif.2013.0241)
50. Bishop PJ, Cuff AR, Hutchinson JR. 2021 How to build a dinosaur: musculoskeletal modeling and simulation of locomotor biomechanics in extinct animals. *Paleobiology* **47**, 1–38. (doi:10.1017/pab.2020.46)
51. Gatesy SM, Manafzadeh AR, Bishop PJ, Turner ML, Kambic RE, Cuff AR, Hutchinson JR. 2022 A proposed standard for quantifying 3-D hindlimb joint poses in living and extinct archosaurs. *J. Anat.* **241**, 101–118. (doi:10.1111/joa.13635)
52. Allen VR, Paxton H, Hutchinson JR. 2009 Variation in center of mass estimates for extant sauriscids and its importance for reconstructing inertial properties of extinct archosaurs. *Anat. Rec. Adv. Integr. Anat. Evol. Biol.* **292**, 1442–1461. (doi:10.1002/ar.20973)
53. Allen VR, Bates KT, Li Z, Hutchinson JR. 2013 Linking the evolution of body shape and locomotor biomechanics in bird-line archosaurs. *Nature* **497**, 104–107. (doi:10.1038/nature12059)
54. Diez Diaz V, Demuth OE, Schwarz D, Mallison H. 2020 The tail of the Late Jurassic sauropod *Giraffatitan brancai*: digital reconstruction of its epaxial and hypaxial musculature, and implications for tail biomechanics. *Front. Earth Sci.* **8**, 1–18. (doi:10.3389/feart.2020.00160)
55. Demuth OE, Wiseman ALA, van Beesel J, Mallison H, Hutchinson JR. 2022 Three-dimensional polygonal muscle modelling and line of action estimation in living and extinct taxa. *Sci. Rep.* **12**, 3358. (doi:10.1038/s41598-022-07074-x)
56. Bryant HN, Russell AP. 1992 The role of phylogenetic analysis in the inference of unpreserved attributes of extinct taxa. *Phil. Trans. R. Soc. Lond. B* **337**, 405–418. (doi:10.1098/rstb.1992.0117)
57. Witmer LM. 1995 The extant phylogenetic bracket and the importance of reconstructing soft tissues in fossils. In *Functional morphology in vertebrate paleontology* (eds JJ Thomason), pp. 19–33. New York: NY: Cambridge University Press.
58. Hutchinson JR. 2002 The evolution of hindlimb tendons and muscles on the line to crown-group birds. *Comp. Biochem. Physiol. A Mol. Integr. Physiol.* **133**, 1051–1086. (doi:10.1016/S1095-6433(02)00158-7)
59. Maddison WP, Maddison DR. 2021 Mesquite: a modular system for evolutionary analysis. See <http://www.mesquiteproject.org>.
60. Allen VR, Kambic RE, Gatesy SM, Hutchinson JR. 2017 Gearing effects of the patella (knee extensor muscle sesamoid) of the helmeted guineafowl during terrestrial locomotion. *J. Zool.* **303**, 178–187. (doi:10.1111/jzo.12485)
61. Irschick DJ, Jayne BC. 1999 Comparative three-dimensional kinematics of the hindlimb for high-speed bipedal and quadrupedal locomotion of lizards. *J. Exp. Biol.* **202**, 1047–1065. (doi:10.1242/jeb.202.9.1047)
62. Sheffield KM, Butcher MT, Shugart SK, Gander JC, Blob RW. 2011 Locomotor loading mechanics in the hindlimbs of tegu lizards (*Tupinambis merianae*): comparative and evolutionary implications. *J. Exp. Biol.* **214**, 2616–2630. (doi:10.1242/jeb.048801)
63. Olberding JP, McBrayer LD, Higham TE. 2012 Performance and three-dimensional kinematics of bipedal lizards during obstacle negotiation. *J. Exp. Biol.* **215**, 247–255. (doi:10.1242/jeb.061135)
64. Delp SL, Anderson FC, Arnold AS, Loan P, Habib A, John CT, Guendelman E, Thelen DG. 2007 OpenSim: open-source software to create and analyze dynamic simulations of movement. *IEEE Trans. Biomed. Eng.* **54**, 1940–1950. (doi:10.1109/TBME.2007.901024)
65. Zaaf A, Herrel A, Aerts P, De Vree F. 1999 Morphology and morphometrics of the appendicular musculature in geckoes with different locomotor habits (Lepidosauria). *Zoomorphology* **119**, 9–22. (doi:10.1007/s004350050077)
66. Allen VR, Molnar J, Parker W, Pollard A, Nolan G, Hutchinson JR. 2014 Comparative architectural properties of limb muscles in Crocodylidae and Alligatoridae and their relevance to divergent use of asymmetrical gaits in extant Crocodylia. *J. Anat.* **225**, 569–582. (doi:10.1111/joa.12245)
67. Dick TJM, Clemente CJ. 2016 How to build your dragon: scaling of muscle architecture from the world’s smallest to the world’s largest monitor lizard. *Front. Zool.* **13**, 8. (doi:10.1186/s12983-016-0141-5)
68. Allen VR, Eley RM, Jones N, Wright J, Hutchinson JR. 2010 Functional specialization and ontogenetic scaling of limb anatomy in *Alligator mississippiensis*. *J. Anat.* **216**, 423–445. (doi:10.1111/j.1469-7580.2009.01202.x)
69. Bates KT, Falkingham PL. 2012 Estimating maximum bite performance in *Tyrannosaurus rex* using multi-body dynamics. *Biol. Lett.* **8**, 660–664. (doi:10.1098/rsbl.2012.0056)
70. Sherman MA, Seth A, Delp SL. 2013 What is a moment arm? Calculating muscle effectiveness in biomechanical models using generalized coordinates. In *Volume 7B: 9th Int. Conf. on Multibody Systems, Nonlinear Dynamics, and Control. Portland, Oregon, 4–7 August*, pp. 1–9: American Society of Mechanical Engineers. (doi:10.1115/DETC2013-13633)
71. Regnault S, Fahn-Lai P, Pierce SE. 2021 Validation of an *Echidna* forelimb musculoskeletal model Using XROMM and diceCT. *Front. Bioeng. Biotechnol.* **9**, 1–25. (doi:10.3389/fbioe.2021.751518)
72. Nesbitt SJ. 2011 The early evolution of archosaurs: relationships and the origin of major clades. *Bull. Am. Mus. Nat. Hist.* **352**, 1–292. (doi:10.1206/352.1)
73. Nesbitt SJ *et al.* 2017 The earliest bird-line archosaurs and the assembly of the dinosaur

- body plan. *Nature* **544**, 484–487. (doi:10.1038/nature22037)
74. von Baczko MB, Desojo JB, Ponce D. 2020 Postcranial anatomy and osteoderm histology of *Riojasuchus tenuisiceps* and a phylogenetic update on Ornithosuchidae (Archosauria, Pseudosuchia). *J. Vertebr. Paleontol.* **39**, e1693396. (doi:10.1080/02724634.2019.1693396)
75. Ezcurra MD *et al.* 2020 Enigmatic dinosaur precursors bridge the gap to the origin of Pterosauria. *Nature* **588**, 445–449. (doi:10.1038/s41586-020-3011-4)
76. Ezcurra MD. 2016 The phylogenetic relationships of basal archosauromorphs, with an emphasis on the systematics of proterosuchian archosauriforms. *PeerJ* **4**, e1778. (doi:10.7717/peerj.1778)
77. Garcia MS, Müller RT, Da-Rosa AAS, Dias-da-Silva S. 2019 The oldest known co-occurrence of dinosaurs and their closest relatives: a new lagerpetid from a Carnian (Upper Triassic) bed of Brazil with implications for dinosauromorph biostratigraphy, early diversification and biogeography. *J. S. Am. Earth Sci.* **91**, 302–319. (doi:10.1016/j.jsames.2019.02.005)
78. Müller RT, Garcia MS. 2020 A paraphyletic ‘Silesauridae’ as an alternative hypothesis for the initial radiation of ornithischian dinosaurs: early evolution of Ornithischia. *Biol. Lett.* **16**, 20200417. (doi:10.1098/rsbl.2020.0417rsbl20200417)
79. R Core Team. 2020 *R: a language and environment for statistical computing*. Vienna, Austria: R Foundation for Statistical Computing. See <https://www.R-project.org/>.
80. Bell MA, Lloyd GT. 2015 strap: an R package for plotting phylogenies against stratigraphy and assessing their stratigraphic congruence. *Palaeontology* **58**, 379–389.
81. Paradis E, Schliep K. 2018 ape 5.0: an environment for modern phylogenetics and evolutionary analyses in R. *Bioinformatics* **35**, 526–528.
82. Revell LJ. 2012 phytools: an R package for phylogenetic comparative biology (and other things). *Methods Ecol. Evol.* **3**, 217–223. (doi:10.1111/j.2041-210X.2011.00169.x)
83. Akaike H. 1974 A new look at the statistical model identification. *IEEE Trans. Autom. Control* **19**, 716–723. (doi:10.1109/TAC.1974.1100705)
84. Otero A, Cuff AR, Allen V, Sumner-Rooney L, Pol D, Hutchinson JR. 2019 Ontogenetic changes in the body plan of the sauropodomorph dinosaur *Mussaurus patagonicus* reveal shifts of locomotor stance during growth. *Sci. Rep.* **9**, 7614. (doi:10.1038/s41598-019-44037-1)
85. Hattori S, Tsuihiji T. 2021 Homology and osteological correlates of pedal muscles among extant sauripsids. *J. Anat.* **238**, 365–399. (doi:10.1111/joa.13307)
86. Carrier DR, Walter RM, Lee DV. 2001 Influence of rotational inertia on turning performance of theropod dinosaurs: clues from humans with increased rotational inertia. *J. Exp. Biol.* **204**, 3917–3926. (doi:10.1242/jeb.204.22.3917)
87. Bishop PJ, Falisse A, De Groot F, Hutchinson JR. 2021 Predictive simulations of running gait reveal a critical dynamic role for the tail in bipedal dinosaur locomotion. *Sci. Adv.* **7**, 1–14. (doi:10.1126/sciadv.abi7348)
88. Gônet J, Bardin J, Girondot M, Hutchinson JR, Laurin M. 2023 Locomotor and postural diversity among reptiles viewed through the prism of femoral microanatomy: palaeobiological implications for some Permian and Mesozoic taxa. *J. Anat.* **00**. (doi:10.1111/joa.13833)
89. Turner ML, Gatesy SM. 2021 Alligators employ intermetatarsal reconfiguration to modulate plantigrade ground contact. *J. Exp. Biol.* **224**, jeb242240. (doi:10.1242/jeb.242240)
90. Berman DS, Sumida SS, Henrici AC, Scott D, Reisz RR, Martens T. 2021 The Early Permian bolosaurid *Eudibamus cursoris*: earliest reptile to combine parasagittal stride and digitigrade posture during quadrupedal and bipedal locomotion. *Front. Ecol. Evol.* **9**, 1–18. (doi:10.3389/fevo.2021.674173)
91. Demuth OE, Wiseman ALA, Hutchinson JR. 2023 Quantitative biomechanical assessment of locomotor capabilities of the stem archosaur *Euparkeria capensis*. Figshare. (doi:10.6084/m9.figshare.c.6398135)